Journal of Nuclear Materials 381 (2008) 137–144

Contents lists available at ScienceDirect

Journal of Nuclear Materials

journal homepage: www.elsevier.com/locate/jnucmat

A structurally-based model of irradiated graphite properties

Mark R. Bradford *, Alan G. Steer

Design Authority, British Energy, Barnett Way, Barnwood, Gloucester GL4 3RS, UK

A B S T R A C T

In this paper, we describe a model of irradiated graphite properties that is based on an understanding of the interconnection of the structure. Simplified conceptual models have enabled us to explain many of the correlations that exist between irradiated graphite material properties and derive mathematical formulations that appear to be of widespread applicability. The principles of the model are illustrated with reference to the irradiation 'structure term' of Young's modulus. It is shown that the currently used definition may be considered to be a combination of three separate processes – pore closure driven densification, increased structural interconnectivity and (latterly) pore generation. It is the structural interconnectivity component that is most closely linked to the changes in other properties such as dimensional change rate and coefficient of thermal expansion, and this relationship is used to direct the mathematical formulations.

1. Introduction

Traditionally, the approach that has been taken when modelling the irradiation behaviour of graphite is to treat each property independently and to define empirical and semi-empirical models for each. However, this approach has led to some notable inconsistencies when attempting to include the effects of influencing factors for which data are sparse. A notable example is the long-standing assumption that radiolytic oxidation affects the irradiation behaviour of dimensional change but not that of the coefficient of thermal expansion (CTE). However, both properties are concerned with the transmission of crystallite driven strain throughout the material microstructure – shrinkage strain in the case of dimensional change and thermal strain in the case of CTE. Therefore, it is reasonable to expect radiolytic oxidation to affect both properties, or neither, but not one in isolation of the other.

It was inconsistencies such as those outlined above, that has led us to reinvestigate the basis of the existing models. The aim of the study is to define models with self-consistent assumptions, based upon a better understanding of the material behaviour as a whole. This will yield improved model reliability when extrapolating beyond the limits of the databases used to derive them. This paper gives an overview of the approach by discussing the role of structural connectivity in the irradiation behaviour, with particular emphasis on the so-called 'structure term' of Young's modulus.

2. A structural approach to graphite properties

2.1. Evidence for the influence of structure in the irradiation behaviour of graphite

When subjected to fast neutron irradiation, the bulk properties of graphite are modified. In near-isotropic graphites, such as that used in the UK advanced gas-cooled reactors (AGRs), bulk shrinkage is accompanied by an increase in Young's modulus, whilst the CTE initially rises then steadily falls (Fig. 1). However, under similar irradiation conditions, the properties of the individual crystals[1] do not undergo any significant change, with the exception of dimensional change [1,2]. In this latter case, growth and shrinkage in the crystallographic *c*-axis and *a*-axis orientations, respectively, is observed (Fig. 2).

Attempts to interrelate the properties by treating the material as an assemblage of crystals (e.g. Simmons, [3]) found some early support in apparently explaining a link between initial shrinkage rate and the CTE. However, this approach breaks down once the material approaches dimensional change 'turnaround' as the change in shrinkage behaviour runs contrary to that predicted from the CTE [4]. More recently Kelly et al. [5] attempted to model the various property behaviours *via* the crystal strain rates and a 'structure term'. Unfortunately, for isotropic material the method relies on the Simmons methodology and was therefore impractical.

In principle, given a computer model that is sufficiently large and representative, with suitable input properties, it should be possible to numerically model the behaviour of the bulk material.

* Corresponding author. Tel.: +44 0 1452 653884; fax: +44 0 1452 652298.
E-mail address: mark.r.bradford@british-energy.com (M.R. Bradford).

[1] Deduced from the behaviour of highly oriented pyrolytic graphite (HOPG).

0022-3115/$ - see front matter © 2008 Elsevier B.V. All rights reserved.
doi:10.1016/j.jnucmat.2008.07.040

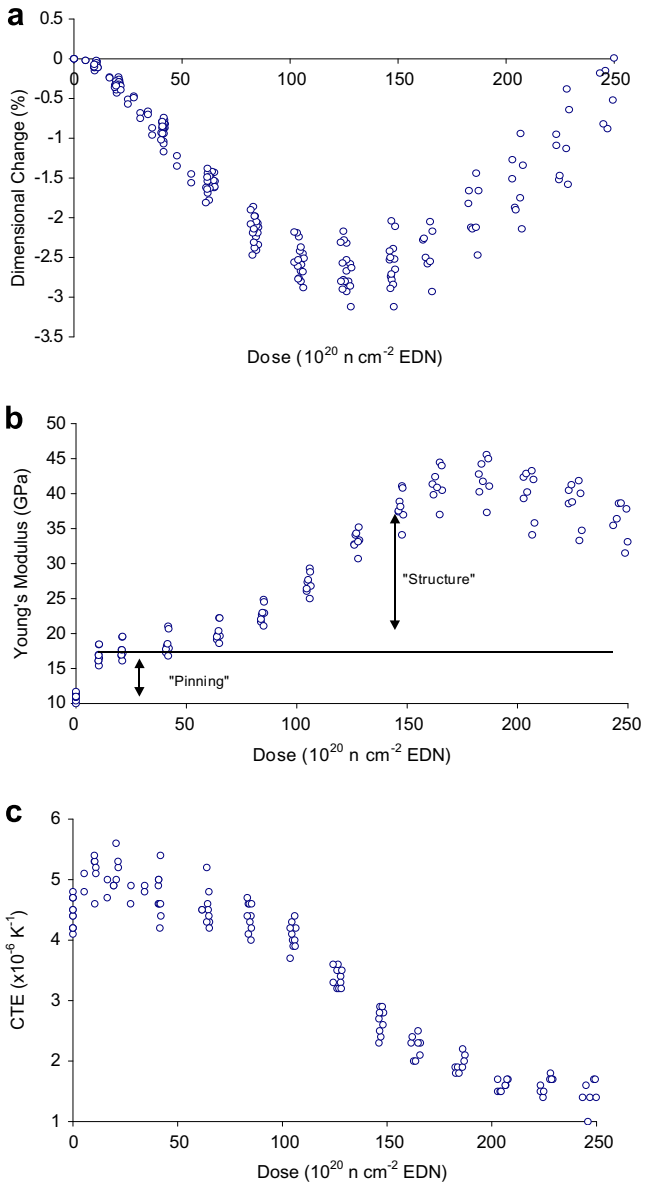

Fig. 1. The behaviour of AGR Gilsocarbon graphites with fast neutron irradiation: (a) dimensional change; (b) Young's modulus; (c) CTE. The irradiation temperature is 430 °C.

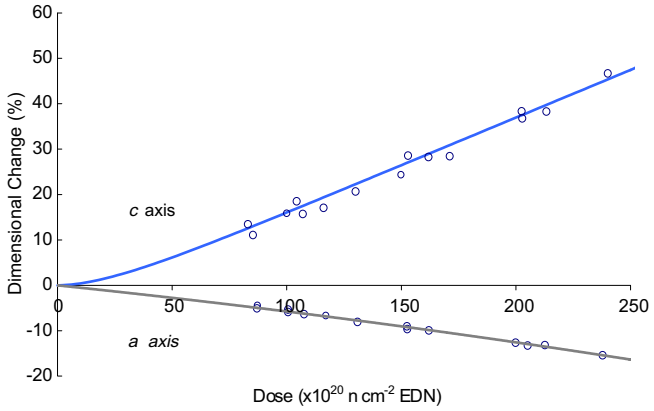

Fig. 2. The dimensional change behaviour of HOPG with fast neutron irradiation (400–700 °C). Data taken from Kelly et al. [2].

One example of such an approach that has met with moderate success is the work of Hall [6]. Unfortunately these approaches are computationally expensive (which restricted Hall's studies to two dimensions) and may ultimately struggle for a lack of representative crystal properties-even the most highly oriented compression annealed pyrolytic graphites are still made up of imperfectly aligned multiple crystals.

We have therefore chosen to adopt a different approach to the problem – that of using analogies and simplified conceptual models to understand how the various components of the structure interact with one another, and hence the ways in which properties are interrelated. The approach is similar to that adopted by Simmons, but extended into three-dimensions. In this way we have been able to define the key relationships that enable improved, physically-based semi-empirical models to be developed.

2.2. The structure of unirradiated graphite

The graphite used in the AGRs is comprised of a Gilsocarbon filler and flour, and a pitch-based binder. The target density was achieved by liquid pitch impregnation (typically two cycles). Following graphitisation, the crystallites appear to be relatively similar in size across the material, whether associated with the filler, binder or impregnant. There are differences in local orientation and ordering of the crystallites within the various regions (Fig. 3) but, on a macroscopic scale, the crystallites are randomly oriented, giving a near-isotropic material.

Interspersed throughout the graphitic phases, there are three principal classes of porosity:

- *Calcination cracks*. Large, lenticular pores formed during the initial coking process. The 'onion-skin' cracks in Gilsocarbon particles are classic examples of calcination cracks.
- *Gas evolution and transport pores*. During the baking of the 'green stock', hydrocarbons and other gases are driven off and form these typically cylindrical aspect-ratio pores.
- *Thermal shrinkage cracks*. At graphitisation temperatures, the atomic motion is facile and the structure is relatively 'fluid', thermal energy allowing bonds to break and reform readily. During cool-down, the structure 'freezes', whereupon the anisotropic crystal CTE, particularly the high *c*-axis CTE, causes local stresses to form. If the stress is high enough, microcracks are formed. These are likely to be of high aspect-ratio and, due to the nature of their formation, will be generally aligned with

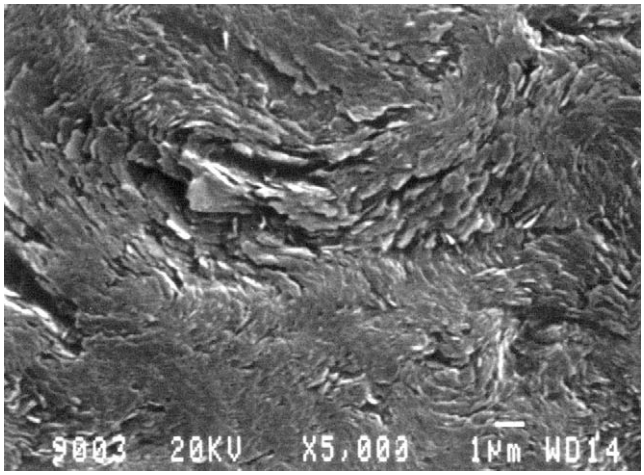

Fig. 3. Scanning electron micrograph of binder phase in Gilsocarbon graphite showing typical crystallite size and the existence of short range order and medium-range disorder.

the crystal *c*-axis. Microcrack initiation at different temperatures during the cooling will result in a distribution of crack sizes and there will still be some residual stress at room temperature in regions of the material where cracking has not occurred.

2.3. The conceptual framework

Within our model framework, we represent the microstructure of the material by a network of ligaments, connected by joints, interspersed with voids/porosity. The ligaments are graphite crystallites or, at a coarser level, domains; the joints are the chemical bonds between the crystallites or domains. The measured bulk properties will be determined by the properties of the component crystals, the nature of the connections between them and, in some cases, by the extent and type of porosity. Where the properties of individual ligaments differ, as in the case of anisotropic graphite crystals of varying alignment, the assessment of the bulk behaviour from the crystal properties must also take into account the action of one ligament upon another. This is a principle well understood in mechanical engineering.

2.4. Application of the conceptual model to the irradiation behaviour of graphite

The application of the concepts of the structural model to the irradiation behaviour of nuclear graphite may be illustrated by considering the '2½ dimensional' structure in Fig. 4, which represents the graphite crystals in their most connected state. Although highly simplified, this is adequate for the present purposes of demonstrating the conceptualisation of bulk behaviour from that of individual components, and the response of the structure to irradiation and radiolytic oxidation. In this representation, the bulk graphite is composed of two parallel plates connected by three ligaments – the inner ligament having a differing material property from the outer two in the stressing direction, because of the differing alignments of graphite planes.

2.4.1. Illustration of the basic principles

2.4.1.1. Young's modulus. The bulk modulus of the composite structure is defined by the strain response for a given load. If a load is applied to the plates in Fig. 4, then all three ligaments will experience equal strain and the greatest stress will be experienced by the ligament(s) of highest modulus. This is a clear illustration of the engineering principle that 'stiffness attracts load'. Further, the 2:1 split of ligament types (crystal alignment) in the illustration enables us to show that the load distribution, and hence the bulk modulus of structure of Fig. 4, will be different according to which of the ligament types is the higher modulus. It therefore follows that the number and relative degree of connectivity of the stiffest ligaments will dominate the bulk modulus of the composite structure. In graphite, the highest modulus is in the plane of the crystals – i.e. the crystallographic *a*-axis.

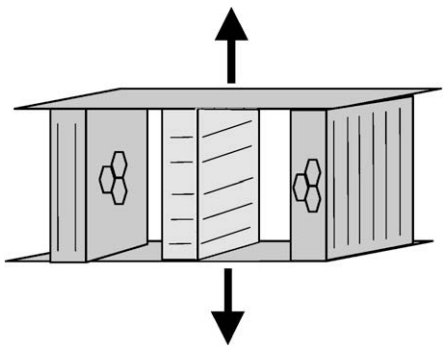

Fig. 4. Schematic representation of a unit within the structural model. The different shades represent ligaments of differing material property.

The illustration also enables us to consider the effect of increasing the porosity within the structure. An increase in the internal porosity can be equated with a reduction in ligament thickness. This reduces the internal load bearing areas, causing the stress in any given ligament to increase for a given external load. If the underlying ligament moduli are unchanged, then the increased ligament stress will result in an increased strain – yielding a reduction in the bulk modulus. The bulk modulus of a graphite specimen will therefore be determined by the underlying crystal moduli, the degree of interconnectivity of the structure and the degree of porosity (i.e. density).

2.4.1.2. Coefficient of thermal expansion. The CTE of the composite structure reflects the equilibrium distribution of internally generated thermal stress, driven by the differing expansion or contraction of the individual ligaments. In graphite, high thermal expansion is observed in the crystallographic *c*-axis, whilst there is negligible expansion (or even contraction) in the *a*-axis. Consequently, in the Fig. 4 illustration, the outer ligaments contract or remain unchanged, whilst the central ligament expands. The result is that the outer ligaments will be placed in tension whilst the inner ligament will be compressed. The net thermal strain of the structure will then depend on the response of each ligament to this self-imposed stress – i.e. it will be a function of the ligament moduli. Since the *c*-axis has significantly lower modulus, it follows that, although the crystal is trying to expand in the c-axis direction, the compressive load imposed upon it by the parallel *a*-axis ligaments constrains the expansion. As a consequence, the bulk CTE of graphite is strongly influenced by the *a*-axis connectivity.

In standard continuum models, CTE is independent of degree of porosity, provided that at least one continuous strand of the network remains intact [7]. Fig. 4 is consistent with this, in that the bulk CTE will be unaffected if the interconnectivity is left intact. The bulk CTE of a graphite specimen will therefore show a strong dependence on the underlying crystal CTE and moduli and the degree of interconnectivity of the crystal structure, but is not likely to be a strong function of the degree or type of porosity.

2.4.2. Application of the concept to the irradiation behaviour of Young's modulus

It has been noted above that irradiation does not fundamentally change the crystal CTE or moduli.[2] However, as Fig. 2 illustrates, it does change the size and shape of the crystals (ligaments) and, consequently, of the porosity. The highly simplified representation in Fig. 4 shows a structure with complete connectivity between the individual ligaments and the plates. In other regions of the microstructure, the thermal shrinkage stresses associated with cooling from graphitisation would have led to microcracking, generating *c*-axis aligned porosity. It is this alignment that enables thermal shrinkage cracks to 'accommodate' the crystal *c*-axis expansion, with the result that the *a*-axis contraction initially dominates, giving the bulk behaviour of Fig. 1(a).

Irradiation also affects the connections between crystals or domains, allowing existing bonds to be broken and reformed and new connections to be made when porosity is closed. It therefore restores to the structure some of the fluidity that exists at graphitisation temperatures. It is this dynamic behaviour that may allow

[2] Seldin and Nezbeda [1] show an increase in c44, but the implied increase in this shear component at the operating temperatures of AGR moderator graphite (~400 °C) is an order of magnitude less than that required to cause a significant change in the bulk modulus of a structure such as that shown in Fig. 4.

the material to undergo irradiation creep when subjected to a stress, whether externally applied or internally generated. Therefore, the observed changes in bulk modulus with irradiation are likely to be the result of a combination of stress relief and structural change.

In the early stages of irradiation, crystal dimensional change rates are slow and there will be little, if any, closure of porosity and increase in connectivity. However, residual internal stress will be relaxed by creep processes. This, and the rebalancing/stiffening of initial connections between crystals and domains should affect the bulk modulus, and experimental evidence suggests that it does – the rapid initial increase generally known as 'Pinning'.

As irradiation proceeds, the rate of *c*-axis growth will increase and the thermal stress cracks will be closed – slowly at first but then at an increasing rate, which some HOPG irradiation data [2] suggest may saturate after an irradiation dose of $\sim 50 \times 10^{20}$ n cm^{-2} (Fig. 2). This crystal shape change drives closure of porosity and an increase in the proportion of the internal load bearing area relative to the bulk, causing the modulus to increase slowly.

With further irradiation, the 'accommodation' porosity is consumed, and the structural interconnectivity increases in three-dimensions. Although not immediately apparent from the highly simplified representation of Fig. 4, this further increases the *a*-axis contribution to the bulk modulus and the rate of rise is more rapid. However, continued *c*-axis expansion will then begin to strain the structural network in the surrounding area. Where this strain cannot be relieved by the breaking and reforming of connecting bonds, new porosity will be generated by microcracking.

Due to the distribution of the pore and crystallite sizes, pore generation will not occur simultaneously and uniformly in all regions of the material. Consequently some regions of the bulk material will still be undergoing pore closure whilst others undergo pore growth. Interestingly, the scale at which these two processes occur is likely to be different: thermal shrinkage microcrack closure will occur throughout the structure, whilst pore growth, being driven by relief of stresses caused by crystal strain, may tend to favour extension of existing cracks and become localised.

Finally, as more aligned cracks are closed, pore generation will increasingly dominate over the pore closure as the effect of the *c*-axis expansion driven pore generation outweighs that of increased interconnectivity, which will saturate as accommodation porosity is consumed. This causes the modulus to first stop increasing, then fall Fig. 1(b)).

This consideration therefore indicates that the development with irradiation of the traditional 'structure term' (Fig. 5) may be considered to be comprised of three components: – pore closure (densification); increased connectivity, which will saturate as accommodation porosity is consumed; and crack/pore formation at higher dose. The identification of the underlying structural connectivity component of modulus is a key aspect of the understanding of the correlation of the irradiation behaviour of graphite properties.

2.5. The role of the structural connectivity term in the modelling of graphite properties

2.5.1. Dimensional change

Kelly and Brocklehurst [8] postulated that the observed bulk dimensional change (as illustrated in Fig. 1(a)) is the result of two processes – an underlying shrinkage and pore generation. It follows that the point of maximum shrinkage – the 'turnaround' point-occurs when the rates of the two processes are equal.

It is evident from the discussion, above, that pore generation and the rapid rise in modulus in the mid-dose region both follow as a consequence of the crystal dimensional change driven closure of accommodation porosity. Therefore we expect to see a strong correlation between the dimensional change pore generation rate and the underlying modulus structural connectivity term. This agrees with experimental data (Fig. 6).

2.5.2. Coefficient of thermal expansion

The conceptual model illustrated by Fig. 4 suggests that there should be a strong negative correlation between Young's modulus and coefficient of thermal expansion – the greater the degree of *a*-axis connectivity, the lower the CTE. This correlation is not clear in the data for unirradiated samples cut from AGR production graphites.

However, the possibility of residual stress on cooling from graphitisation temperatures has been raised in an earlier section, and it is known that an externally applied elastic strain modifies the bulk CTE [9]. Consequently, it is possible that not only will the unirradiated CTE not fully reflect the underlying structure of the material, the observed increase in CTE at low-dose (Fig. 1(c)) may be the result of the relief of residual cooling stress. A similar process has been postulated as a contributor to the 'pinning' component of Young's modulus. This suggests that there should be a stronger negative correlation between the CTE and the modulus after the initial relaxation of cooling residual stress, and before the pore closure-induced increase in modulus occurs. Such a correlation is seen within the available data once any density differences between individual samples have been accounted for (Fig. 7).

It has also been noted above that, with increasing dose, the crystal shape change drives the closure of porosity without significantly increasing the structural interconnectivity. The CTE will therefore, to first order, be unaffected[3] during this phase. However, as the dose increases further, and the accommodation porosity is consumed, the interconnectivity increases in three-dimensions. As a result, the influence of the *a*-axis will increase and the bulk CTE is expected to fall. Therefore we expect to see a strong negative correlation between the CTE and the underlying modulus structural connectivity term. Again, this is in full agreement with the experimental data (Fig. 8).

By contrast, pore generation due to continued *c*-axis expansion is likely to have little effect on bulk CTE. The high dose increase in porosity is likely to be dominated by growth of existing cracks and pores and, since the connectivity in material around the pores will remain largely unaltered, the continuum theories of CTE behaviour will apply. Consequently, the interconnectivity model also predicts that the fall in CTE should not be continual, but should asymptote, as can be seen in Fig. 1(c).

2.5.3. Strength

As noted by Marsden et al. [10], it has been common practice in the nuclear industry to equate the change in strength with irradiation, $\Delta\sigma$, to the square root of the change in modulus, ΔE. This has been rationalised by reference to the Griffith criterion, which is intrinsically related to the fracture surface energy in a crystal. However, operational evidence suggests that this assumption tends to underestimate the increase in strength and Marsden et al. note that other power relationships (between square root and linear) are observed. This is particularly the case where trends with porosity (density) are investigated. The conceptual model illustrated by Fig. 4 provides a physically-based explanation for these observations.

Our illustration of the basic principles behind the structural model suggests that the effect of an increase in porosity is to reduce the internal load bearing area causing the stress in any given

[3] Interestingly, a consideration of the relative changes of the shapes of the crystals, and hence contact areas, suggests that the CTE should fall slightly during the early densification phase as relatively more of the contact area is made up of *a*-axis aligned material, increasing the contribution of that component.

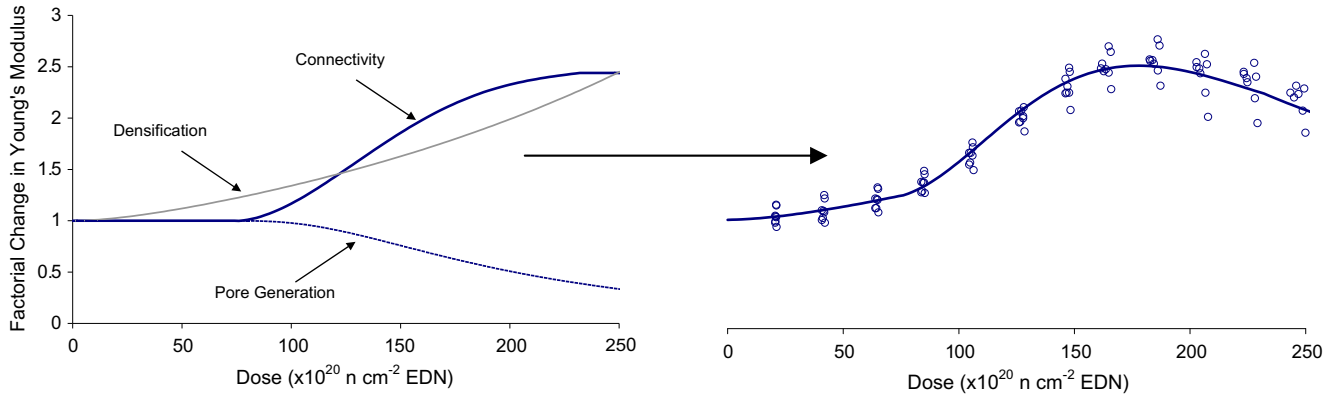

Fig. 5. The construction of the Young's modulus 'structure term' from its separate components.

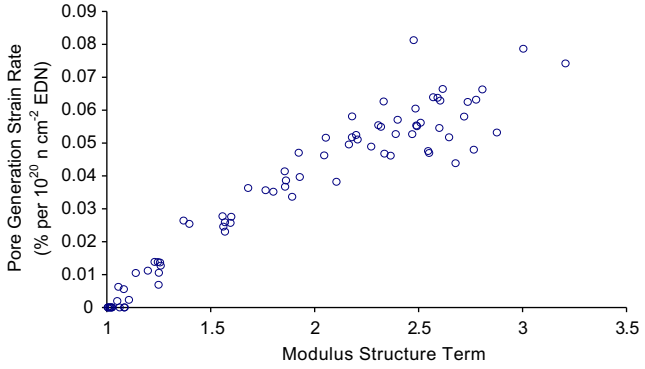

Fig. 6. The correlation between the dimensional change pore generation rate and the Young's modulus structural connectivity term.

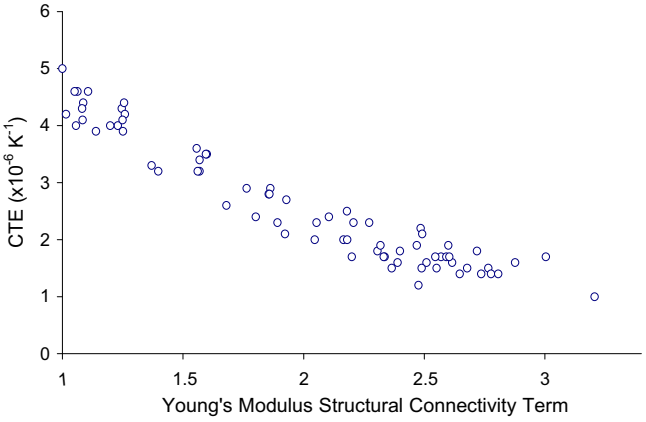

Fig. 8. The correlation between the CTE and the Young's modulus structural connectivity term.

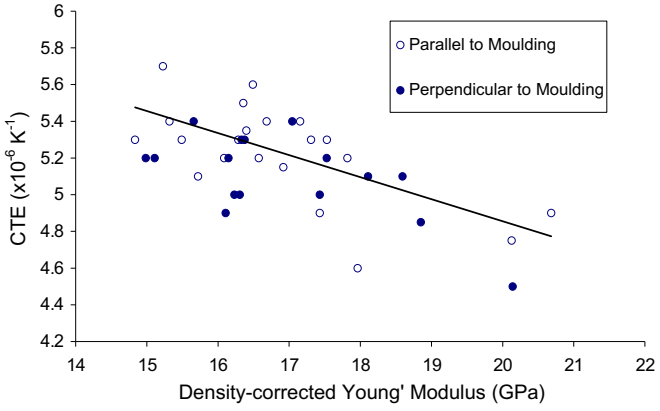

Fig. 7. The correlation between CTE and Young's modulus at low-dose.

ligament to increase for a given load. The same principles can be applied to a porosity change that is induced by crystal shape change, i.e. the densification and pore generation terms of Fig. 5. For bulk porosity changes (e.g. weight loss, sequential impregnation), a linear relationship between the change in modulus and the change in strength is more usually observed [10].

Similarly, we are of the opinion that irradiation 'pinning' involves more than one process, one of which is stress rebalancing and relief throughout the structure. Stress relief processes would yield an improvement in the strength without significant change to the modulus, indicating that the net $\Delta E - \Delta\sigma$ power relationship for irradiation pinning is likely to be greater than square root. Furthermore, only the underlying structural connectivity term can, in concept, be related to changes in the crystal network that would align with the premise of the Griffith criterion and would be therefore expected to demonstrate a square root relationship between ΔE and $\Delta\sigma$. Therefore, our modelling framework strongly suggests that the combination of pinning, structural connectivity and porosity changes will lead to a net power dependence for the $\Delta E - \Delta\sigma$ relationship that is greater than square root but less than unity.

3. Description of the mathematical framework

The significant changes in dimensions, modulus, CTE and strength are all driven by the underlying crystal dimensional change and the corresponding increase in structural interconnectivity. This, in turn, is driven by the closure of the accommodation porosity. Therefore, the fundamental basis for any mathematical framework should be:

- A representation of the underlying (crystal) dimensional change rate.
- A representation of the accommodation porosity distribution.

Supplemented by:

- Connectivity-pore generation strain rate (dimensional change) or connectivity-CTE relationships.
- Densification and pore growth descriptions (E, strength).

3.1. The underlying (crystal) dimensional change

Here we use a modification of the notation previously employed by Kelly and Burchell [5], where the dimensional change of the polycrystal was denoted G_x, the underlying shrinkage was based on the crystal shape change parameter X_T, and the volume increase due to the generation of new porosity (the pore generation strain) was denoted F_x. In our notation, we denote the underlying shrinkage as G_u and retain the pore generation term, F_x, thus:

$$\frac{dG_x}{d\gamma} = \frac{dG_u}{d\gamma} + \frac{dF_x}{d\gamma} \tag{1}$$

Fig. 2 suggests that the rates of change of the crystal dimensions gradually increase to a saturation level. Other HOPG data [11] suggest that a more parabolic behaviour may be appropriate. We have examined the HOPG data available and note a strong dependence of the behaviour on the heat treatment temperature. We further note that the gradual increase to linear behaviour appears to be the more widespread for well graphitised material. Consequently we have chosen to represent the HOPG behaviour, and therefore the underlying shrinkage, with the following form (used to produce the fitting lines in Fig. 2):

$$\frac{dG_u}{d\gamma} = A \cdot (1 - e^{-k_1\gamma}) \tag{2}$$

where A and k_1 are constants controlling the magnitude and saturation dose, respectively.

3.2. Accommodation porosity and structural connectivity

The increase in structural interconnectivity is driven by the closure of the accommodation porosity and therefore can be modelled by an 'accommodation pore' size distribution, combined with a description of the rate of closure. However, for ease of application, we currently combine these two factors into a direct description for the structural connectivity term, which we denote S_C. The connectivity term has an 'S-curve' shape, and we find that a standard distribution function of the normal or log-normal type provides an adequate description of the behaviour, i.e. (for the normal distribution case):

$$S_C(\gamma) = B \cdot \int_{y=0}^{\gamma} \left(\frac{1}{\sqrt{2\pi}\sigma} \cdot e^{-\left[\frac{(y-\mu)^2}{2\sigma^2}\right]} \right) \cdot dy \tag{3}$$

where μ and σ are, respectively, the mean and standard deviation of the (in this case) normal distribution function and B is a scaling factor that determines the magnitude of the connectivity term.

The example given here is for the case where the 'pinning' and structural connectivity terms are all combined additively. However, Eason et al. [12] demonstrate that for the case where the terms are combined factorially, the approaches are algebraically equivalent if the structure term (here, the connectivity term) is defined as

$$S'_C(\gamma) = 1 + S_C(\gamma)/P \tag{4}$$

where P is the low-dose saturated value of the irradiation pinning term.

3.3. Connectivity-pore generation strain rate relationship and bulk dimensional change

We find that, with the structural connectivity term described as above, a good description of the pore generation strain rate, and hence the overall dimensional change behaviour, is obtained using the following relationship, as follows:

$$\frac{dF_x}{d\gamma} = C \cdot S_C(\gamma) \cdot \frac{dG_u}{d\gamma} \tag{5}$$

where C is a constant that determines the magnitude of the pore generation strain rate. The term in G_u is included to allow for the case where pore closure occurs whilst the underlying shrinkage rate has not reached saturation. For the practical cases shown below, saturation is complete before S_C begins to be significant and Eq. (5) effectively reduces to a simple linear relationship. The bulk dimensional change is then given by integration of Eq. (1).

3.4. Connectivity-CTE relationship

We find that a simple linear relationship is also adequate to describe the relationship between the structural connectivity and the CTE_{20-120}, as follows:

$$\frac{CTE_\gamma}{CTE_{sat}} = 1 - D \cdot S_C(\gamma) \tag{6}$$

where D is a constant and CTE_{sat} is the low-dose 'residual stress annealed' CTE_{20-120}.

3.5. The effect of densification and pore generation on Young's modulus and strength

It is assumed that the Young's modulus densification and pore generation terms, G_E and F_E, respectively, can be modelled using standard exponential, Knudsen-type, relationships, as follows:

$$G_E = e^{-\beta_G \varepsilon_G} \tag{7}$$

$$F_E = e^{-\beta_F \varepsilon_F} \tag{8}$$

where β_G and β_F, and ε_G and ε_F, are the respective Knudsen relationship constants and fractional volume changes associated with the underlying shrinkage and pore generation. The Young's modulus at dose, γ, is then given by

$$E_\lambda = E_0 \cdot (P + S_C(\gamma)) \cdot G_E \cdot F_E \tag{9}$$

and the strength is given by

$$\sigma_\lambda = \sigma_0 \cdot \sqrt{(P + S_C(\gamma))} \cdot G_E \cdot F_E \tag{10}$$

Equivalent formulations to Eqs. (9) and (10) can be drawn up for the case where P and $S_C(\gamma)$ are combined factorially.

We have chosen to retain the assumption that the strength is dependent on the square root of the 'pinning' term while further investigations are carried out into the this component of the irradiation behaviour. However, since or model indicates that the actual power dependence may be greater than square root, we expect the current formulation to lead to a small, but systematic, bias towards lower predicted strength than is observed.

4. Discussion

4.1. Application to experimental data

To date, the equation framework has been tested against data from the following graphite sources across a range of temperatures of applicability to both current and future operating reactors. The comparisons include:

- Gilsocarbon based 'pre-production' material
- Gilsocarbon based 'AGR production' material
- US and German HTR grade materials (H-451 and ATR-2E).

The comparisons have been carried out by an iterative-linear least squares fitting to the data. The order of fitting has been:

underlying shrinkage rate (Eq. (2)), wider dimensional behaviour (Eqs. (3) and (5)), then Young's modulus (Eqs. 3, 7, and 8, with iteration on Eq. (5) due to an implicit coupling) and finally CTE (Eq. (6)). The strength behaviour is a genuine prediction based on the constants derived for modulus. These initial comparisons suggest that the equation framework is of widespread applicability. However, for brevity we present the results of only two comparisons:

Fig. 9(a)–(d) presents the results of the comparison against the Gilsocarbon pre-production grade PI-6 obtained in Dounrey Fast Reactor DFR at around 400 °C [13]. PI-6 is the Gilsocarbon graphite grade for which the most extensive dataset exists across all four properties on the same samples. In particular, this is one of the most complete materials test reactor strength datasets that exist for Gilsocarbon graphites.

The scatter in the measured properties is high. This is in part due to variations in the irradiation temperatures of the various samples. Nevertheless, it can be seen that the form of Eqs. (1)–(10) provides a very good description of the trend in the data and captures the key behaviours, including the suggestion that the form of Eq. (10) introduces a slight systematic bias into the prediction of irradiated sample strength.

Fig. 10(a) and (b) presents the comparison against the data for HTR grade ATR-2E, irradiated at 500 °C, which were presented at the first International Graphite Specialists Meeting (INGSM-1) [14]. Although data for only two properties (dimensional change and modulus) are available, the scatter in measurements is considerably less than for the PI-6 grade, and provides a better visual comparison of the capability of the modelling framework.

The level of agreement achieved against the experimental data is highly encouraging,

At present, the approach described here is semi-empirical – the equations are firmly rooted in a physical understanding of the underlying material behaviour, but the precise predictions for any given graphite grade require some data to aid in the determination of the appropriate constants. A wider comparison with experimental data should allow us to identify which of the fitting parameters are constants, which vary according to the graphite grade and whether any changes to the equation framework are necessary to enable the model to be fully predictive. Nevertheless, whilst this development continues, the physical basis for the descriptions increases the confidence in the ability of the model to make predictions beyond the limits of the dataset. This is particularly beneficial where full and prototypic data are scarce – as in the case of simultaneous irradiation and radiolytic oxidation.

4.2. The influence of radiolytic oxidation

In contrast to its thermal counterpart, which is predominantly limited to the gas transport porosity, radiolytic oxidation acts throughout the whole of the open porosity within the structure. The processes that control radiolytic oxidation act in such a way that it is most efficient in small, slab shaped pores, and favours the corrosion of the outermost planes of a crystal [15]. Both of these aspects come together to suggest that open thermal shrinkage cracks will be oxidised efficiently in such a way as to increase the available accommodation porosity. From the discussion presented here, it can be seen that this would be expected to lead to a delay in shrinkage turnaround, for which there is clear evidence in support from material test reactor experiments [16].

However, since it is the closure of the accommodation porosity that leads to the increase in structural connectivity, $S_C(\gamma)$, radiolytic oxidation is now expected to delay the onset of any phenomena that are linked to this term – specifically the rapid increase in modulus at moderate dose and the accompanying fall in CTE.

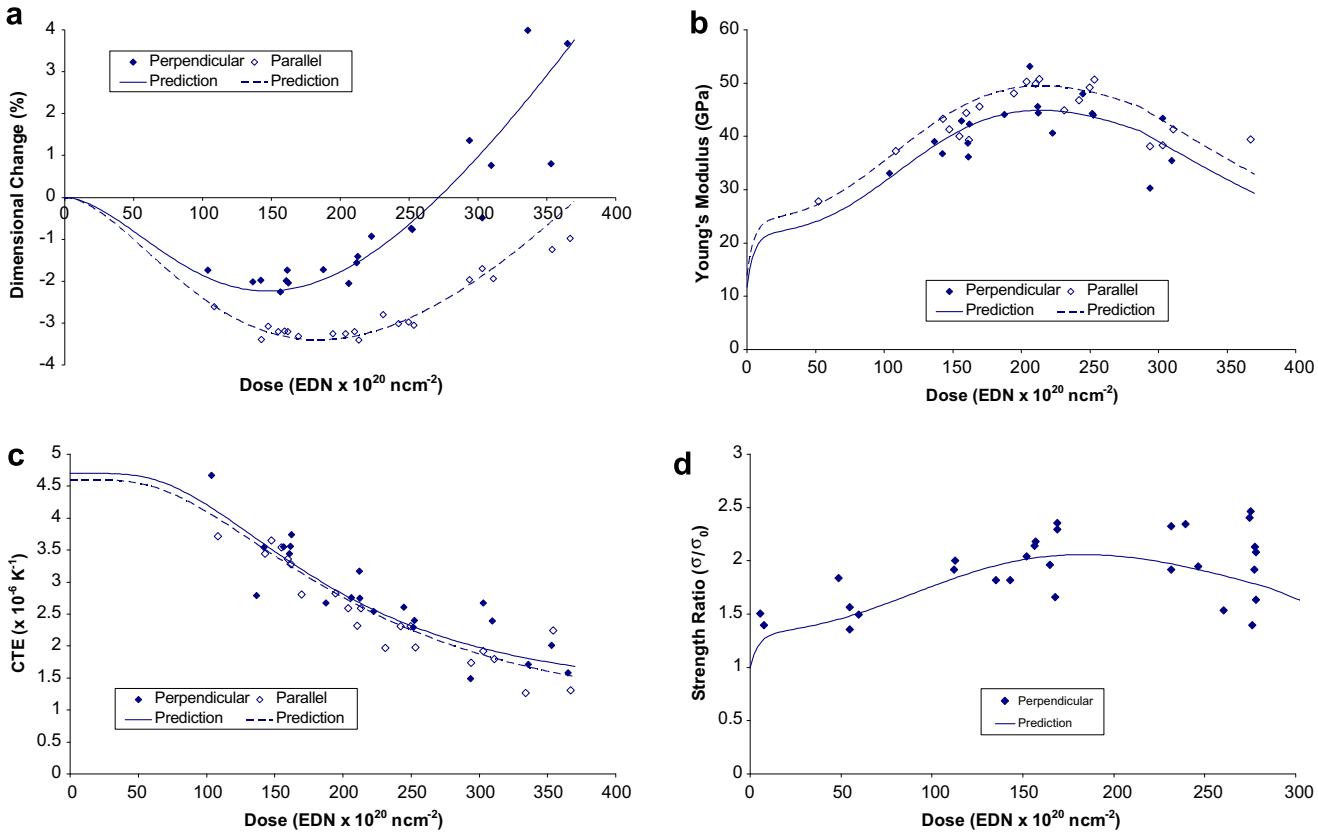

Fig. 9. Comparison of observed and predicted behaviour for graphite grade PI-6 at ~400 °C: (a) dimensional change; (b) Young's modulus; (c) coefficient of thermal expansion; (d) strength.

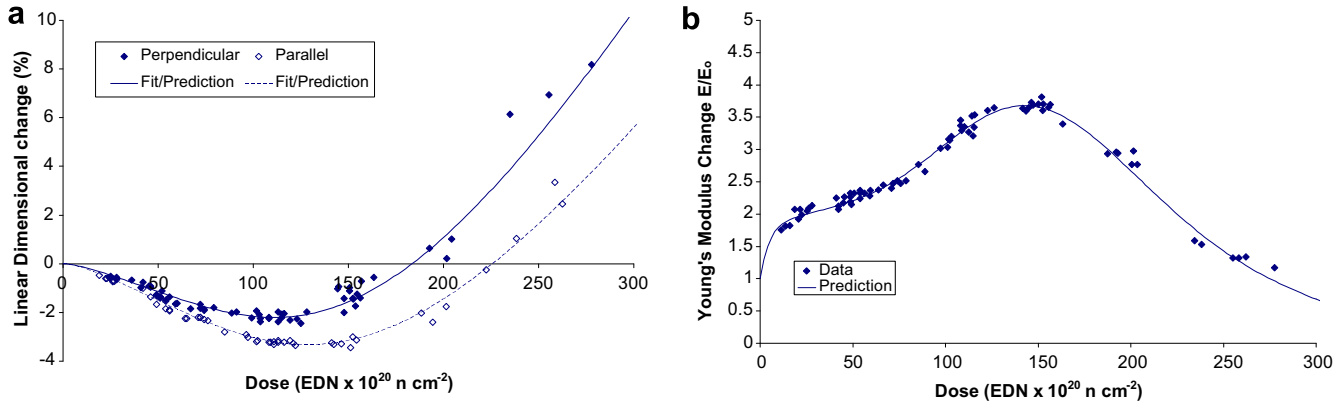

Fig. 10. Comparison of observed and predicted behaviour for graphite grade ATR-2E at 500 °C: (a) dimensional change; (b) Young's modulus.

Information in support of both of these predictions is beginning to be obtained from the operating AGR reactors.

The prediction in respect of the behaviour of CTE is particularly significant since there is evidence that neither radiolytic [17] or thermal [7] oxidation has any significant effect on the CTE of unirradiated graphite. This is consistent with the continuum models of CTE [7], as discussed earlier in this paper. The significant advance made by the structural model presented here is that the effect of radiolytic oxidation on the irradiation induced change to the continuum can now be identified and reconciled with emerging information.

4.3. Summary of current position

The modelling described here has therefore achieved our initial goal of designing improved framework models with self-consistent assumptions that are consistent with often seemingly disparate experimental data. This increases the confidence in the ability of semi-empirical models to make reliable predictions beyond the limits of the database used in their derivation. The next phase of our investigations will focus on the fitting constants and whether there are clear interactions between them that will enable us to take the equation framework and generate a model that is genuinely predictive.

5. Conclusions

A model of the behaviour of irradiated graphite has been developed, based on an understanding of the interconnection of the crystallites within the structure. The approach has enabled the identification of the most significant correlations that exist between certain of the properties.

It has been shown that the currently used definition of the 'structure term' of Young's modulus can be considered to be a combination of three separate processes – pore closure driven densification, increased structural interconnectivity and (latterly) pore generation. The structural interconnectivity component of modulus is closely linked to the changes in other properties such as dimensional change rate and coefficient of thermal expansion and may be used to define self-consistent models for the simultaneous irradiation and oxidation behaviour of these three properties.

Acknowledgement

The authors would like to thank British Energy Generation Ltd for permission to present this paper.

References

[1] E.J. Seldin, C.W. Nezbeda, J. Appl. Phys. 41-N8 (1970) 3389.
[2] B.T. Kelly, J.E. Brocklehurst, Carbon 9 (1971) 783.
[3] J.H.W. Simmons, Radiation Damage in Graphite, Pergamon Press, Oxford, 1965.
[4] B.T. Kelly, W.H. Martin, P.T. Nettley, Philos. Trans. A 260 (1966) 37.
[5] B.T. Kelly, T.D. Burchell, Carbon 32-N3 (1994) 499.
[6] G.N. Hall. Microstructural modelling of nuclear grade graphite. EngD Thesis, University of Manchester, 2005.
[7] P.J. Hacker, G.B. Neighbour, B. McEnaney. The coefficient of thermal expansion of graphite. Bath Nuclear Materials Group report, 1999, BNMG/REP/024, United Kingdom HSE Reference FC/GNSR/44.
[8] B.T. Kelly, J.E. Brocklehurst. Dimensional changes in graphite at high radiation doses and the effects of continuous radiolytic oxidation. UKAEA report TRG-M-5967(S), 1971, See [13].
[9] S.D. Preston, B.J. Marsden, Carbon 44 (2006) 1250.
[10] B.J. Marsden, S.L. Fok, T.J. Marrow, P.M. Mummery, in: Proceedings of HTR-2004, Second International Optical Meeting on High Temperature Reactor Technology, Beijing, 22–24 September 2004.
[11] J.E. Brocklehurst, B.T. Kelly, Carbon 31-N1 (1993) 179.
[12] E.D. Eason, G.N. Hall, B.J. Marsden, G.B. Heys, these Proceedings.
[13] UKAEA – Various reports written between 1947 and 1996, available from the UK public records office http://www.pro.gov.uk, filed under section AB.
[14] G. Haag. in: Presentation to the first International Nuclear Graphite Specialists Meeting, Oak Ridge, Tennessee, September 5, 2000.
[15] J.V. Best, W.J. Stephen, A.J. Wickham, Progress in Nuclear Energy 16-N2 (1985) 127.
[16] B.T. Kelly, J.E. Brocklehurst, B.W. Ashton. The interaction of radiolytic oxidation and fast neutron irradiation in the moderators of CO_2 cooled reactors. UKAEA report TRG 2589(S), 1974. See [13].
[17] J.E. Brocklehurst, R.G. Brown, K.E. Gilchrist, V.Y. Labaton. The effect of radiolytic oxidation on the physical properties of graphite. UKAEA report TRG 1712 (C), 1968. See [13].